Abnormal grain growth and Fe/Mn stained fluid paths in metacarbonates of the Damara Orogen (Namibia)

C. J. Gross, K. Weber, S. Siegesmund and A. Vollbrecht

Institut für Geologie und Dynamik der Lithosphäre, Universität Göttingen, Goldschmidtstr. 3, D-37077 Göttingen, Germany

Coarsely crystalline metacarbonates exhibiting post-metamorphic exaggerated grain growth fabrics and evidence for hydrothermal alteration have been investigated by means of various methods (e.g. thin section analysis, cathodoluminescence microscopy and the electron microprobe). Each rock type, consisting of graphite-bearing sparry calcite marbles and sparry dolomite marbles, exhibits a complete transitional fabric development from host rock to marbles showing exaggerated grain growth. The final stage in the coarsening process leads to the growth of sparry calcite rhombohedral blasts and sparry dolomite porphyroblasts. The dominant mechanism in the sparry calcite marble is grain boundary migration, whereas the sparry dolomite marble formed by a combination of solid state processes (coalescence crystallization) and hydrothermal processes. The driving force behind this process is the reduction of interfacial free energies, leading to an increase in grain size and a reduction of the grain boundary surface area. Grain-scale fluid-rock interaction resulting from the infiltration of Fe-/Mn-rich fluids created a very complex series of cathodoluminescence fabrics in the sparry dolomite marbles. Unique zonation assemblages, formed by diffusion processes and solution/precipitation occur all along the grain boundaries and microcracks. These form an interconnected Fe-rich network and attest to extensive and active material transport. The gradual and abrupt changes in the Fe and Mn contents point to cyclical or episodic fluid influxes.

Introduction

A wide spectrum of terms are found in the literature describing the phenomenon of grain growth, in which some grains in a monomineralic material grow faster at the expense of a matrix with the same composition. In metals, Hillert (1965) and Porter and Easterling (1981) describe this process as abnormal grain growth. Detert (1978) suggests grain growth during secondary recrystallization which has been used by Stöckhert and Duyster (1999) to describe the grain growth fabrics in recrystallized quartz veins. In these phenomena, grain boundary migration is the dominant mechanism. Grain boundary migration is generated by the difference in free energy across a curved boundary. The difference in free energy makes a grain boundary move towards its center of curvature, causing grain size reduction in small aggregates and size increases in large aggregates (Tullis and Yund, 1982). The radius of curvature of a grain face is directly proportional to the diameter of the grain. Thus, the driving force and rate of grain growth is directly proportional to grain size. Kingery *et al.* (1976) defined this relation as follows:

$$D - D_o = kt^n$$

Where D equals the mean grain diameter at a time t, D_o is the mean initial grain size, k is a constant dependent on temperature and grain boundary mobility and n is the growth exponent with an average value of 0.4. Growth rate not only depends on the driving force, but also on grain boundary mobility (Tullis and Yund, 1982). The presence of other phases or impurities can cause a reduction in the grain boundary mobility (Porter and Easterling, 1981).

The phenomenon of exaggerated grain growth often observed in metals and ceramics has direct application to geologic materials. This is especially the case with the fabric development and extreme grain size growth observed in the metacarbonates from the two study areas in the Damara Orogen. The two areas were chosen because they developed under contrasting metamorphic conditions and the geologic formations to which they belong show evidence for extensive hydrothermal processes and material transport by fluids (e.g. skarn mineralization in the Karibib Formation and silicification, albitization and tourmalinization in the Corona Formation). The contrasting materials (calcite and dolomite) also have different physical properties and responded differently to the exaggerated grain growth. The microstructures observed attest to a high grain boundary mobility, especially in the graphite-bearing sparry calcite marbles. The presence of calc-silicate minerals in the sparry calcite marble act like impurities in metals causing a reduction of grain boundary mobility.

Geologic Setting and Field Relations

The Damara Orogen belongs to the Upper Protero-

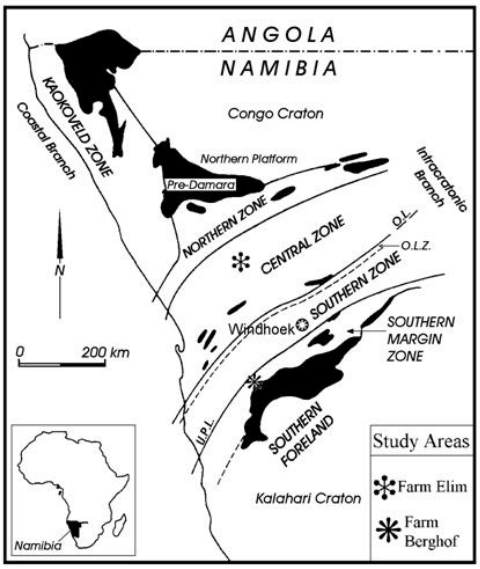

Figure 1: Simplified map delineating the tectonostratigraphic zones in the Damara Orogen, Namibia (Miller, 1983; map from Henry *et al.,* 1990). The location of the two sample sites is shown on the map. O.L. = Okahandja Lineament; O.L.Z = Okahandja Lineament Zone; U.P.L. = Us Pass Lineament.

zoic to Lower Paleozoic (900-450 Ma) Pan-African mobile belt system. Three main structural divisions (the Northern, Central and Southern Zone) are used to delineate the Damara Orogen based on lithologic, metamorphic and tectonic considerations (Miller, 1983; Fig. 1). The two metacarbonate samples collected for this study consist of a graphite-bearing calcite marble from the Karibib Formation (northern Central Zone, CZ) and a metadolomite from the Corona Formation (Southern Margin Zone, SMZ; Fig. 1).

Metamorphic grade gradually increases from the south and north in the Damara Orogen and reaches high-grade amphibolite conditions in the CZ. Using dolomite-calcite solvus thermometry, Puhan (1983) determined a pressure range of 3 - 4 kb with temperatures ranging from 590 - 660°C. Abrupt changes in the P-T conditions develop south of the Okahandja Lineament Zone. In the SMZ, Puhan (1988, 1995) investigated the assemblage tremolite + talc + calcite + dolomite + quartz in siliceous dolomites on the eastern side of the Aris-Rietfontein basement complex. Two temperature groups were determined: (1) a high T range from 545 - 583°C where tremolite occurs and (2) a low T range of 476 - 522°C where talc develops. Pressure conditions reached 6-9 kb.

The Karibib Formation forms an extensive carbonate unit in the Central and Northern Damara Belt. It was subdivided by Klein (1980) into three members: (1) the basal Harmonie Member which is predominantly a calc-silicate rock, with minor calcitic marbles and schists, (2) the middle Otjongeama Marble Member which consists of light grey calcite-dolomite marbles that include minor calc-silicate layers and (3) the Aresis River Member (ARM), a coarsely crystalline, graphite-bearing calcite marble which exhibits an exaggerated grain growth fabric and the development of large sparry calcite rhombohedra. This type of exaggerated grain growth represents a post-metamorphic phenomenon and is not restricted to the ARM. It can be found in all marble units in the CZ of the Damara Belt. However, it is generally most spectacularly developed in the ARM.

On Farm Elim (Fig. 1), the development of exaggerated grain growth fabrics occurs in exposures of the ARM along the road from Usakos to Uis approximately 5 km south of the Omaruru River near Nainais. The largest sparry calcite rhombohedra (>10 cm) appear to be confined to the western edge of the exposure, specifically at Farm Elim. The calcite rhombohedra decrease in size and number away from the Farm Elim outcrops where the ARM only exhibits a coarsely crystalline grain fabric. A complete grain size distribution can be observed in the coarsely crystalline calcite marble (grain sizes 0.5 mm to >1 cm), and then a relatively radical jump to the large sparry calcite rhombohedra. Figure 2 shows an example of the exaggerated grain growth fabric present in the ARM exposures at Farm Elim. A sharp contact is at first observable between the two grain size domains (1 and 3 being the coarse-grained graphite-bearing calcite marble and 2 representing the sparry calcite rhombohedra; Fig. 2). Upon closer inspection, the contact between these domains appear less sharp, reflecting the irregular and interpenetrating grain boundaries between the abnormally grown calcite and the coarse-grained graphite-bearing calcite marble. The concentration of graphite is most prevalent in the coarse-grained marble, in contrast to the sparry calcite where it occurs sporadically or in many cases is lacking (Fig. 2).

The Corona Formation represents a transgressive shallow marine carbonate and siliciclastic facies which stratigraphically forms the base of the Swakop Group at the northwestern margin of the Kalahari Craton. It consists of calcitic and dolomitic marbles, metasandstones, metaconglomerates, metaquartzites, phyllites, muscovite-biotite schists and subordinate iron formation. The stratigraphic position of the formation is complex due to the shallow marine shelf environment superimposed by

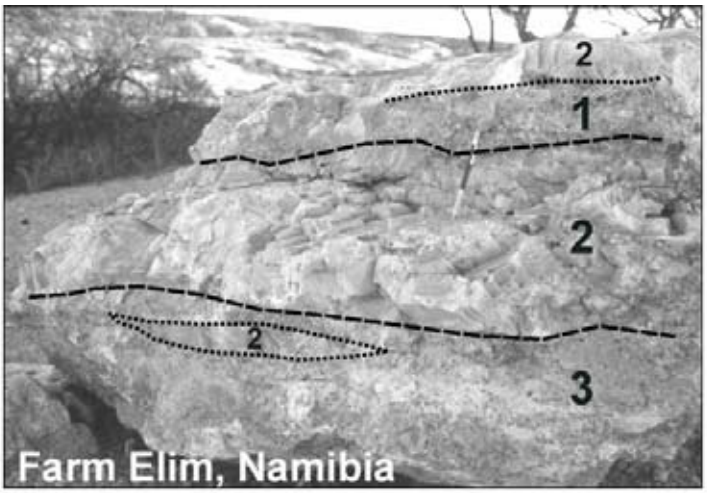

Figure 2: Outcrop exposure exhibiting the exaggerated grain growth fabric in the graphite-bearing calcite marble (Karibib Formation – ARM) at Farm Elim. Areas designated with the numbers *1* and *3* represent coarse-grained marble consisting of calcite, graphite and calc-silicate minerals. Graphite is evenly distributed throughout these areas. Abnormally large calcite occurs in the areas marked with the number *2*.

glacio-eustatic sea level changes resulting in large lateral variations in lithology and thickness ranging from a few meters to 2 000 m (Weber and Vietor, 1996).

In the area of the farm Berghof (Fig. 1), the Corona Formation consists of the following rock types: brown siliceous dolomite, white siliceous dolomite, medium-grained dolomite marble with sparry dolomite porphyroblasts, talc-bearing dolomite and a medium to dark blue-grey dolomite mylonite. They range in thickness from 20 - 50 m, in which dominantly the top 3 - 10 m have been strongly hydrothermally altered. The most distinctive feature of this alteration zone is the growth of large sparry dolomite porphyroblasts (1cm to >10cm) which are embedded within a relatively pure dolomite marble exhibiting a grain size of 0.5 mm to 4 mm. Figure 3 depicts the sparry dolomite marble. The sparry dolomites occur as isolated porphyroblasts, in clusters or can be totally lacking from the dolomite marble. The weathered out sparry dolomites exhibit their characteristic rhombohedral cleavage. Detailed descriptions of the other rock types are given in Gross *et al.* (1999). The blue-grey dolomite mylonite, however, is interpreted as being the host for the grain-coarsened dolomites, lying stratigraphically below the hydrothermally altered and coarsened metadolomites listed above. The rock mainly consists of fine-grained dolomite, quartz, relict calcite and minor plagioclase, phlogopite and graphite. Thin quartzitic layers exhibit tight isoclinal folds.

Field evidence for hydrothermal events are present in the form of large hydrothermal quartz veins cross-cutting the metacarbonates. These quartz veins also contain very large euhedral dolomite crystals ranging from a few cm to >30 cm in size. Sporadic alteration (bleaching indicated by changes of colour from reddish brown to white) occurs in the blue-grey dolomite mylonite, with sharp and gradational contacts between altered and unaltered rock. The alteration is associated with fractures (1 - 2 m long and 10 - 15 cm wide) and tension fissures that have been filled with a hydrothermal vein dolomite. Thin veins of quartz also occur.

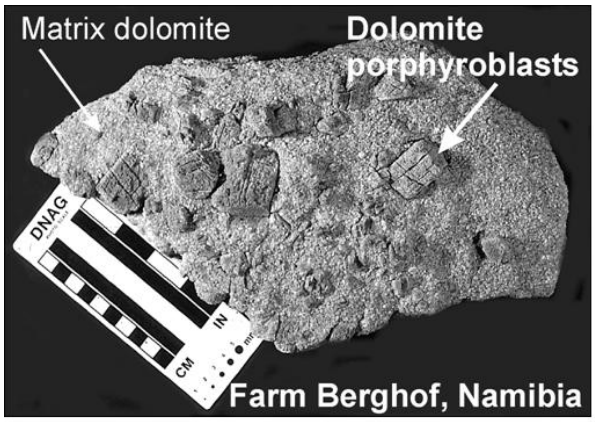

Figure 3: Sparry dolomite marble from the Corona Formation, Farm Berghof. Large sparry dolomite porphyroblasts are embedded in a medium-grained dolomite marble.

Analytical Methods

The two metacarbonate samples exhibiting the unique grain growth fabrics described in this study were investigated with the petrographic microscope, by cathodoluminescence microscopy (CL), back-scatter electron imaging (BSE) and chemically analysed with the electron microprobe. Neutron texture analysis was also performed on the dolomite marble with the sparry dolomite porphyroblasts using the SKAT texture diffractometer in Dubna, Russia. Details of the method are given in Ullemeyer *et al.* (1998).

The type of "hot-cathode" CL microscope used for this study is the HC3-LM apparatus developed in Bochum, Germany which uses as its base an Olympus BHMJ microscope (see Neuser *et al.*, 1995). The operating conditions under which these samples were observed are: specimen vacuum chamber 0.001 mbar, filament current 160-170 mA and an accelerating potential 14 kV. The advantage of using a CL microscope of this type is that it allows the investigator to observe the sample with reduced transmitted light (TrL) and the CL input. Initial investigations with the "cold-cathode" method (Neuser *et al.*, 1995) did not reveal as much detailed information as the "hot-cathode" method. With the "cold" CL method the Fe-rich grain boundary zonations in the medium-grained dolomite matrix and in the dolomite porphyroblasts, were only visible as very dark zones. Further differentiation of the Fe-rich zonation is possible with the "hot" CL method, allowing the differences in Fe concentration to be qualitatively visible. Detailed descriptions concerning the method and principles behind CL microscopy are given in Marshall (1988) and Barker and Kopp (1991).

Quantitative analyses on the two metacarbonate samples were conducted using a JEOL-JXA-8900AL electron microprobe. The carbonates were analysed for Ca, Mg, Mn, Fe, Sr and Ba using the following standards: wollastonite, MgO, rhodochrosite, Fe_2O_3, coelestine and barite. Feldspars were analysed for Si, Al, Na, K and Ti along with the elements listed for the carbonates. BSE images were made on both samples and on this basis detailed chemical profiles across mineral grains, grain boundaries and growth zonations were completed. Operating conditions were: an accelerating voltage of 15 kV, a beam current of 12 nA and a beam size of 5 µm (focused). For further information on the techniques of electron microprobe analysis and BSE imaging see Reed (1996).

Microfabric Observations

Farm Elim – Karibib Formation (ARM)

An overview of selected microstructures and grain fabrics in the sparry calcite marble is shown in Figs. 4A-H. The thin section images shown here are interpreted as successive stages in the continuous grain growth

process. Calcite exhibits a wide variety of microstructures. The process of grain coarsening begins in a calcite marble exhibiting a fabric with equilibrium triple-point grain boundaries, representing an earlier metamorphic fabric. These can be found as relicts with sharp and straight boundaries in the coarse-grained marble (Fig. 4A). The beginnings of grain boundary migration takes place with the dismantling of triple-point boundaries and the formation of finely serrated, irregular grain contacts (Fig. 4B). Some of the surrounding grains in Figure 4B have completely lost their previous grain shape. When the process of grain coarsening is taken a step further, the rock develops a fabric where the calcite grains exhibit irregular grain shapes characterized by serrated, interpenetrating grain boundaries. Figure 4C depicts highly irregular grain shapes of coarse-grained calcite, where the direction of grain boundary movement is indicated by the arrows. The large white arrow points to a twin-free bulge (a low energy state), migrating into a neighboring calcite grain with higher dislocation densities. This represents the best indication for the direction of the migrating boundary front, (e.g. the absence of substructures such as twins and subgrains behind the migrating front). Migration can also occur along and laterally outward from a twin boundary (Fig. 4D), indicating the altion of dislocation densities. Another example of the direction of grain boundary movement can be seen in Figure 4E in which the right grain is growing across the twin lamellae of the neighboring grain. Some microstructures observable can be interpreted as leftover grains, further indicating direction of grain growth. The structure shown in Figure 4F is interpreted as representing the development of a leftover grain as the grain at extinction coalesces around the "mushroom-shaped" lobe. As the grain boundary migration proceeds, the leftover grains are formed as shown in Figure 4G. The direction of the migrating front can be discerned by the fact that the leftover grain (arrow) has the same twin at extinction as the parent grain. The grain enclosing the leftover grain is also relatively twin-free.

Graphite occurs as thin flakes along the grain contacts between coarse calcite grains, in small clusters and sporadically as inclusions in the large sparry calcites. In the coarse-grained calcite, graphite is evenly distributed throughout the marble, with grain sizes of 3 - 4 mm. Graphite also encloses fine- to medium-grained calcite. Closer inspection of these calcite grains reveal small clusters of fluid inclusions in the grain interior. As the grain contacts with graphite are approached, the fluid inclusions decrease. Graphite can hinder or terminate a migrating calcite grain boundary but only at the local grain scale (Fig. 4H). Calc-silicate minerals occur both in thin layers or in clusters. Where they occur in greater concentration, grain coarsening is hindered. The calc-silicates consist of anhedral quartz, diopside, scapolite and chondrodite.

The CL observations of the sparry calcite marbles are summarised in Table 1. In general, the CL colours for these rocks range from very dark brown to reddish brown and reddish orange. Some of the sparry calcite marbles show completely homogeneous CL colours with no indications of fluid-related alterations. A representative example of the "cold" CL fabric in the coarse-grained, graphite-bearing calcite marble is shown in Figure 5A. Internal chemical zonations are usually visible in the calc-silicate minerals such as scapolite and diopside (Fig. 5B). In none of the coarse calcite grains or in the sparry calcites investigated were growth zonations visible. Areas of high luminescence are visible near the graphite, in the vicinity of the zoned calc-silicate minerals and in some areas that closely follow the grain boundaries and microcracks (Fig. 5B). A slightly higher luminescence also outlines some twin planes. Zonation structures do occur in the sparry calcite marbles but only as a direct consequence of a later cataclastic overprinting of the ARM. Hydrothermal fluids participating in these events created veins cross-cutting the sparry calcite marble rock fabric.

Farm Berghof: Corona Formation

The overall rock fabric of a complete thin section

Table 1: Cathodoluminescence observations in the graphite-bearing calcite marbles of the Karibib Formation (Farm Elim).

Rock Material	CL Colours	Characteristic Features
White coarse-grained sparry calcite marble	Calcites exhibit homogeneous red-brown to brown CL colours Calc-silicates show diverse CL colours: greens, blues, light yellow and light brown	Very poor CL to good CL in calcite grains Calc-silicate minerals and inclusions show very good to strong CL, show zonations and alteration processes Thin fluid pathways visible along some grain boundaries No zonations visible in the coarse-grained calcite or in the sparry calcite
Grey coarse-grained sparry calcite marble	Calcites exhibit homogeneous dark brown to brown to reddish brown CL colours	Very poor CL to good CL in calcite grains Relatively good to strong CL in calc-silicate minerals; some zonations Relatively good CL along microcracks and near graphite flakes No zonations observable in the coarse-grained calcite or the grey sparry calcite
White calcite mylonite	Brown CL colours Strong red-brown colours along microcracks Blue to beige CL colours in calc-silicates	No CL to poor CL to relatively good CL Few calc-silicate minerals show good CL Fluid pathways; no CL zonations observable A very fine-grained mylonite: almost no CL to poor; no CL microstructures
Calcitic marble cataclasite	Reddish-brown CL colours	Good CL; material is very fine-grained and exhibits lots of CL structures only visible along grain boundaries Light CL in the twin lamellae

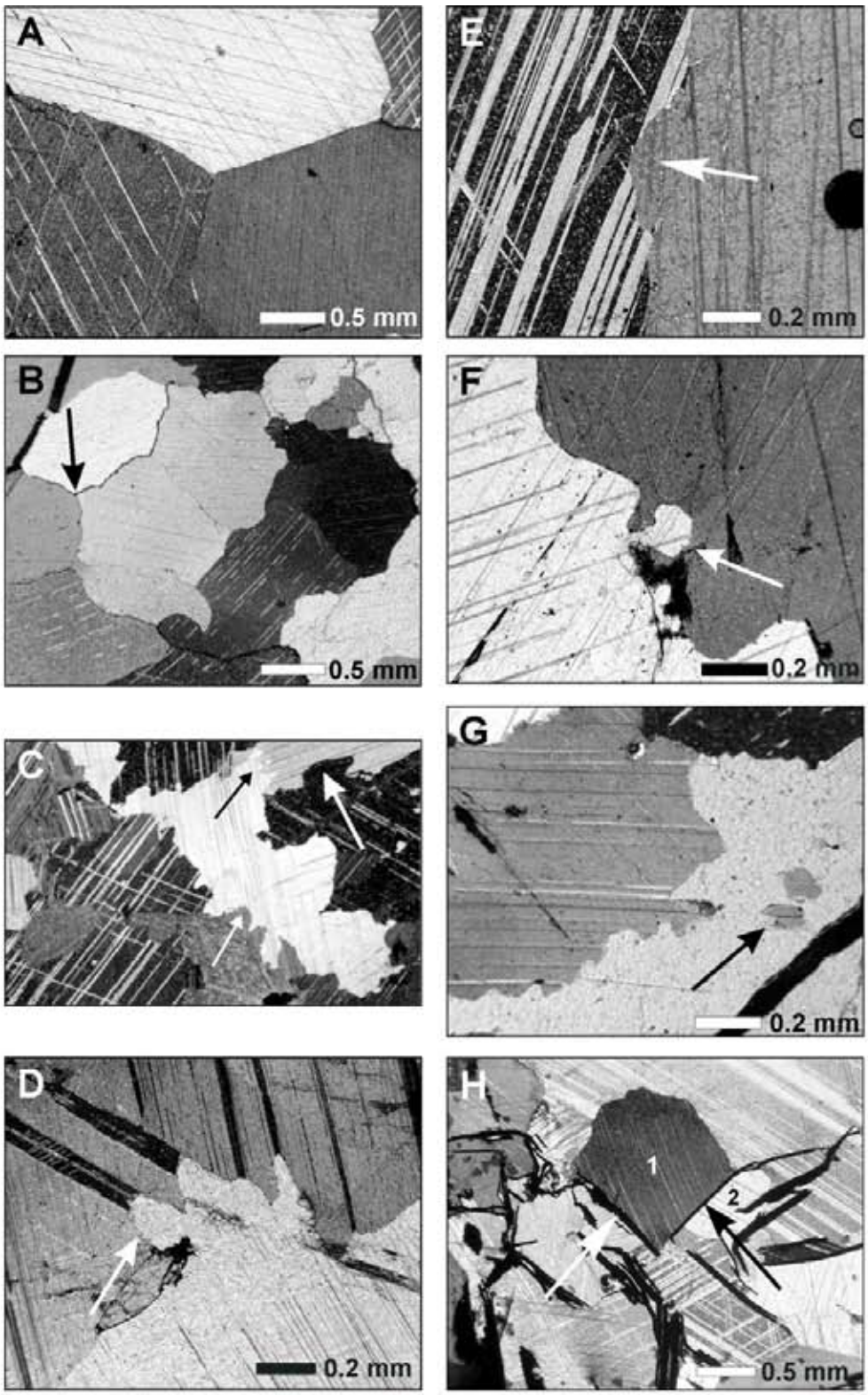

Figure 4: Photomicrographs of representative microstructures and grain boundary configurations in the coarse-grained graphite-bearing calcite marble. (A) Relic triple-point grain boundary with sharp and straight grain contacts. (B) Triple-point geometry showing initial stages of grain boundary migration. Arrow points to triple-point junction and the irregular nature of the grain contacts. Cf. Fig. 4A. (C) Highly twinned calcite grains exhibiting serrated and bulbous grain boundaries. Arrows indicate direction of grain boundary movement. Photo width = 2.2 mm. (D) New grain growth moving selectively into specific twin boundary domains (arrow). (E) Close-up of two calcite grains in which direction of grain boundary movement is indicated by the bulging of the right grain (arrow) across the twins of the left grain. (F) Close-up of the development of a left-over grain by the process of pinching. (G) Possible leftover grains indicating grain boundary migration from the right. (H) Graphite flakes (arrows) acting as a local hindrance to GBM. This relationship is evident between calcite grains 1 and 2.

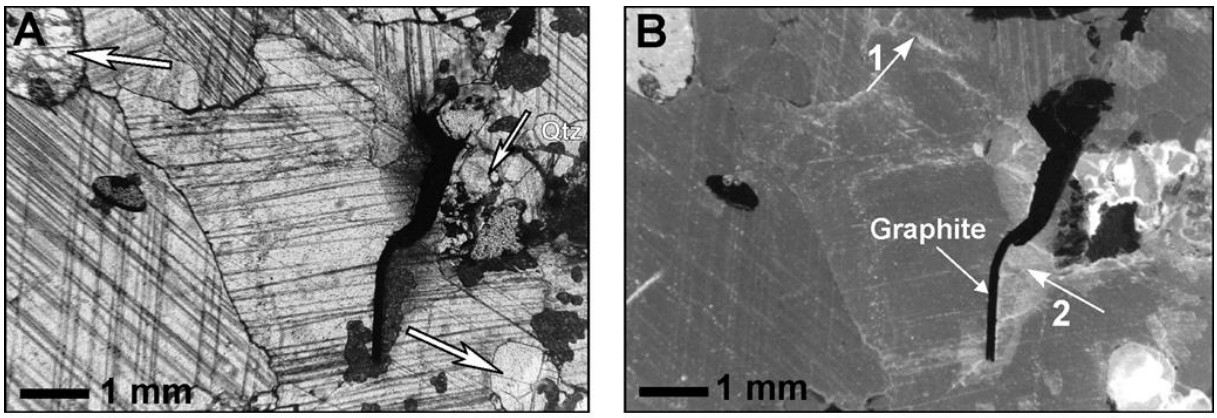

Figure 5: Representative CL fabrics observable in the coarse-grained graphite-bearing calcite marble of the ARM (Farm Elim). (A) Twinned coarse-grained calcite marble in transmitted light (TrL). Arrows point to calc-silicate minerals. Minor quartz is also present. (B) Corresponding CL image. Overall the coarse-grained calcite marble and the abnormally grown calcite show homogenous CL colours. Arrows 1 and 2 point to areas along the grain boundary and near the graphite flake that exhibit lighter CL colours. This is interpreted as probable secondary fluid influence. The calc-silicate minerals show homogenous CL colours and are in some instances zoned with a bright bluish rim and white cores (right-hand side of image).

depicting the medium-grained dolomite marble with the sparry dolomite is shown in Figure 6A. The matrix dolomite exhibits a shape preferred orientation as indicated by the white line. Dolomite matrix grains range in shape from flattened (a small percentage) to elongated "augen-shaped" grains of variable width. A few have irregular shapes. They range in size from <1 mm to 4 mm giving the matrix a relatively homogeneous grain size. Grain boundaries in the matrix can be straight or have very fine irregularities. The matrix consists of pure dolomite (about 97%) with minor accessories comprising albite, talc and pyrite.

The large sparry dolomites show their rhombohedral habit when they weather out of the matrix but their shape appears anhedral in thin section (Fig. 6A). They contain a relatively large volume of very fine-grained to fine-grained inclusions (mostly visible when the sparry dolomite is at extinction) consisting of albite clusters, talc, quartz and pyrite. Often the sparry dolomite exhibits parallel microcrack arrays. Boundaries interpreted as sub-grains or former grain boundaries are also discernible in the sparry dolomites (arrow in Fig. 6A). The interface or contact zone between the dolomite matrix and the sparry dolomite is usually irregular and fluent as shown in Figure 6A, area 1. A close-up of area 1 is depicted in Figure 6B. Visible is an angular embayment of matrix grains extending into the sparry dolomite at area 1. A few small grains (indicated by the black arrow) can be followed from the indentation tip as grains enclosed by the growing sparry dolomite (Fig. 6B). These are interpreted as possible leftover grains.

The bulk texture analysis with the neutron diffractometer revealed that the medium-grained dolomite matrix shows a good lattice-preferred orientation. The c-axis and a-axis pole figures are shown in Figure 7.

Evidence for Fluid-Rock Interaction

Evidence for extensive grain-scale fluid-rock interaction is visible in the sparry dolomite marble. Table 2 summarises the CL observations. Figure 8A depicts the medium-grained dolomite matrix in reduced transmit-

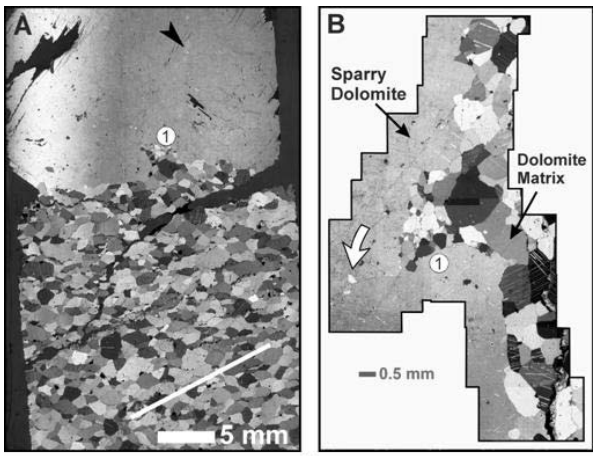

Figure 6: (A) Photomicrograph mosaic of the complete fabric between the medium-grained dolomite matrix and a sparry dolomite porphyroblast. (B) Close up of area 1 shown in image (A).

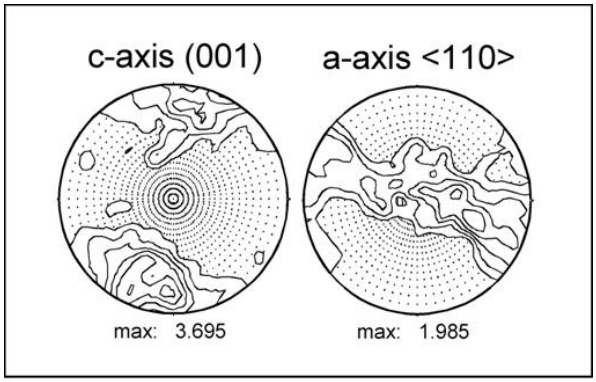

Figure 7: a-axis and c-axis pole figures from the dolomite matrix depicted in Fig. 6. Lower hemisphere, stereographic projection, lowest contour equal to 1.0 multiples of random distribution. Maximum given below pole figure.

Table 2: Cathodoluminescence observations in the sparry dolomite marble of the Corona Formation (Farm Berghof).

Rock Material	CL Colours	Characteristic Features
Dolomite porphyroblasts	Yellow-orange colour in Fe-poor areas Various shades of brown in Fe-rich zones	Fine-grained albite inclusions are zoned – blue rims and dark cores – only associated with Fe-rich zones Fe-rich zones show curvilinear embayments or as subrounded isolated zones in a 2-d section Fe-rich zones cut across parallel microcracks & large sectors of the porphyroblast Minor rhythmical growth zonations only detectable with BSE
Medium-grained dolomite matrix	Yellow-orange colour in Fe-poor areas Various shades of brown in Fe-rich zones parallel grain boundaries	No zoning present in matrix albite Interconnected network of Fe-rich zones parallel grain boundaries Some matrix grains exhibit a slightly darker core Rhythmical growth zonations sometimes present in grain boundary areas

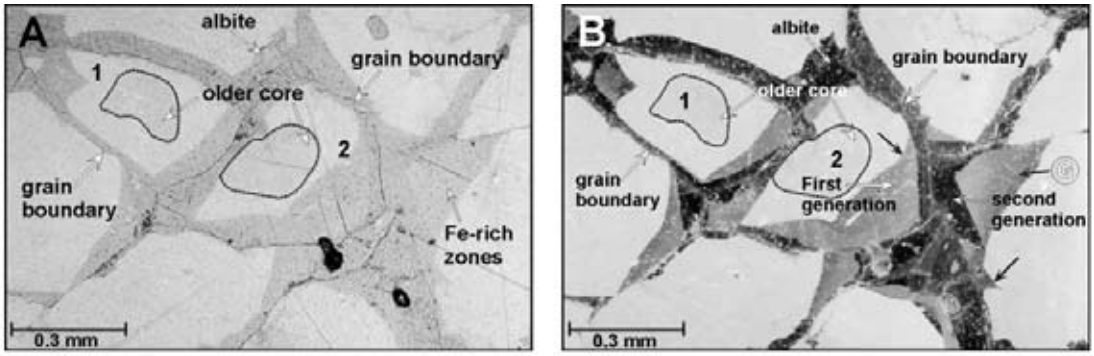

Figure 8: (A) Thin section image combining reduced TrL and CL in the medium-grained dolomite marble. Grain boundaries are easily discernible along with the Fe-rich grain boundary zonation. Dolomite grains 1 and 2 exhibit cores with slightly darker luminescence. These occur sporadically in the marble and are interpreted as representing older cores. Albite, which is generally associated with the Fe-rich zones, is indicated by an arrow. (B) Corresponding CL image of the medium-grained dolomite marble exhibiting the complex, interconnected Fe-rich grain boundary zonations. Two generations of Fe enrichment are discernible. (G) indicates an area of gradational luminescence in the first generation. The black arrows point to sharp, somewhat curvilinear or angular zone boundaries.

ted light (TrL). The corresponding CL image shows the complexity of the Fe-rich zones (Fig. 8B). The Fe-rich zones along the grain boundaries form an interconnected network. This Fe-rich network is present regardless of the plane in which a section is taken. Some of the smaller grains can be completely altered but the larger grains (0.5 - 4 mm) show that the Fe-rich zones extend into the grains over variable distances. Zonation boundary morphology varies considerably throughout the rock fabric (black arrows in Fig. 8B). Furthermore, the Fe-rich zone boundaries deviate significantly from the grain boundaries (grains 1 and 2 in Fig. 8A and 8B). Two distinct Fe-rich zones, a lighter zone with apparent luminescent gradations and a much darker zone, are evident along the grain boundaries (Fig. 8B). The relationship between these two distinct Fe-rich zones is an overlapping one. Rhythmical growth zonations showing alternating bands of various CL intensities sometimes occur in the Fe-rich zones along the grain boundaries (see BSE image in Fig. 12).

The CL fabrics in the sparry dolomites are similar to those observed in the medium-grained dolomite matrix. The Fe-rich zonations represent former fluid pathways cutting across large sectors of the sparry dolomite porphyroblasts. In Figure 9, a CL photo mosaic depicts the characteristic Fe-rich alteration zones observable in the sparry dolomite. Large Fe-rich alteration zones and a very fine network of Fe-rich staining along microstructures (black arrows), interpreted as former matrix grain boundaries, occur in the sparry dolomite (Fig. 9). The large alteration zones are subdivided into a first and second generation based on differences in Fe concentration as in the matrix dolomite. The first generation (labelled 1) forms the lighter zonation, whereas the second generation forms the dominant alteration zone (no. 2) and almost completely covers the first phase of Fe infiltration. Associated with the Fe-rich alteration are zoned albite grains, occurring as isolated grains along the Fe-rich former grain boundary network or in clusters within the larger alteration zones. These enrichment zones are also connected to the network in the dolomite matrix. Under CL this is visible where the Fe-enriched former

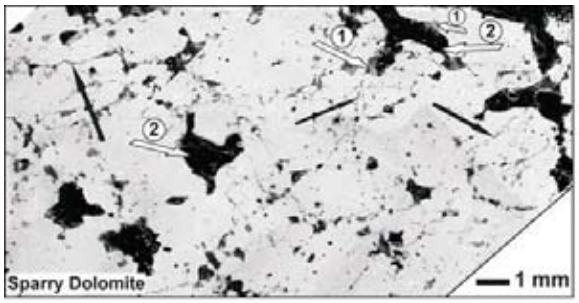

Figure 9: CL mosaic image of the sparry dolomite porphyroblast. Black arrows point to former matrix dolomite grain boundaries. Arrows (1) and (2) point to the first and second generation of Fe-rich fluid influx.

fluid pathway occurs at the contact zone between the dolomite matrix and dolomite porphyroblasts. Zonation related to crystal growth or similar to those often observed in the pore-filling cements of sedimentary carbonates have not been observed in the large dolomite porphyroblasts.

Electron Microprobe Analyses

Farm Elim – Karibib Formation (ARM)

The calcite grains measured with the electron microprobe come from the transition zone between the abnormally-grown calcite and the coarse-grained, graphite-bearing calcite marble. The chemical profile depicted in Figure 10 shows that the composition through a coarse calcite grain is relatively homogeneous. The same results (not shown) were obtained through a large abnormally-grown calcite grain. Fe and Mn contents are extremely low or below the detection limit, whereas Sr has a similar concentration to Mg from point 1 to 20. Only at the points 22-28 is a discernible change in composition evident. In this part of the calcite grain, the CaO content decreases as the MgO content increases. Furthermore, BaO shows higher detectable levels than either FeO and MnO. The BSE image above the profile in Figure 10 also indicates a homogeneous composition in that no distinct zonations or alteration by fluids are indicated. The two lighter grains at the left are calcite grains with a different orientation. The low CaO value at point 1 and the sharp MgO drop at point 31 may be due to its proximity to a grain boundary and a cleavage plane, respectively.

Farm Berghof – Corona Formation

The BSE images of the medium-grained dolomite marble are in good agreement with the data obtained from the CL microscope. The BSE image shown in Figure 11 depicts in greater detail the distribution of the various Fe concentrations along the grain boundaries and the extent of former fluid infiltration into the dolomite grains. Complex zonations that were too fine in detail to be observed with the CL microscope can be seen in dolomite grain 2 (arrow no. 2, Fig. 11). The profile in Figure 11 is separated into specific zones (*A*-*E*) where the grain is unaltered or exhibits distinct chemical changes. In zones *A* and *E*, the FeO and MnO contents are very low corresponding to the luminescent parts of the grains. The regions labelled *B*, *C* and *D* exhibit an increase in the FeO content and a simultaneous rise in the MnO content, although its level is much smaller in comparison. The incorporation of Fe and Mn in the dolomite structure is also associated with a concurrent decrease in the CaO content and a somewhat larger decrease in the MgO content as is very evident in zone *B* (Fig. 11).

Quantitative analyses conducted across the rhythmic growth zones in the medium-grained dolomite marble are shown in Figure 12. The profile is divided into distinct zones (*A*-*G*) which correspond to the chemical changes visible in the BSE image above. In the BSE mode, considerable detail and complexity is observable, such as thin and straight zonation and wider bands which have irregular boundaries. The most irregular zone boundary occurs between the luminescent part of the grain and the zone with the lightest gray value, i.e., with the highest Fe concentration (zone *B*). The next growth band beginning with analysis point 30 (zone *C*) also shows some boundary irregularity but more closely conforms to the general pattern of the thin growth zonations.

From left to right on Figure 12, the FeO concentration appears highest (>2.0 wt.%) in zone *B*. A gradual decrease in the FeO content occurs in growth band *C*. Small fluctuations appear in the thin rhythmical growth zonations in area *D*. The FeO concentration rises again in area *E* and then begins declining towards the grain boundary. Similar drops take place in the MgO and CaO content at the grain boundary. The increase in the

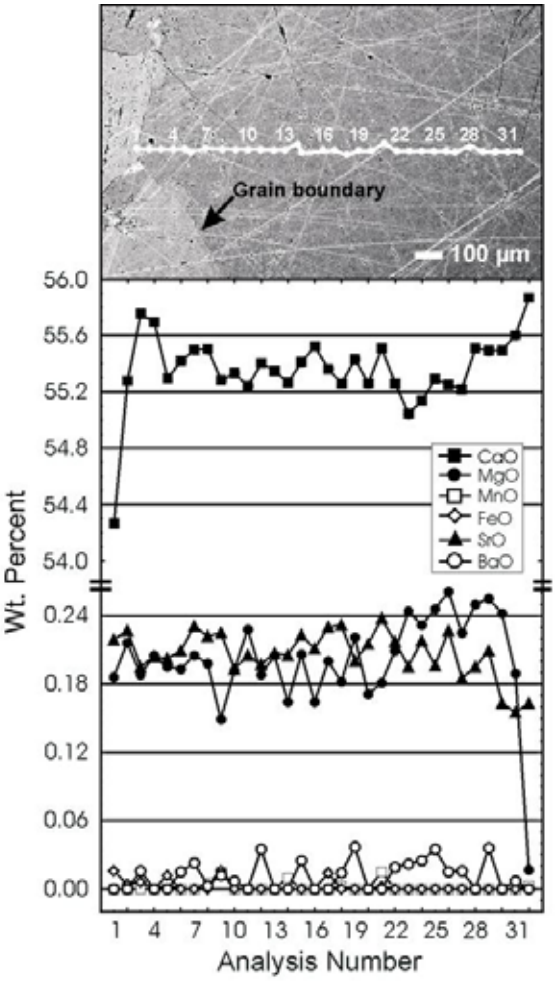

Figure 10: Electron microprobe analysis with corresponding back-scatter electron (BSE) image across a large calcite grain in the graphite-bearing calcite marble of ARM (Farm Elim). The phase contrast of the grain to the left is due to its different orientation.

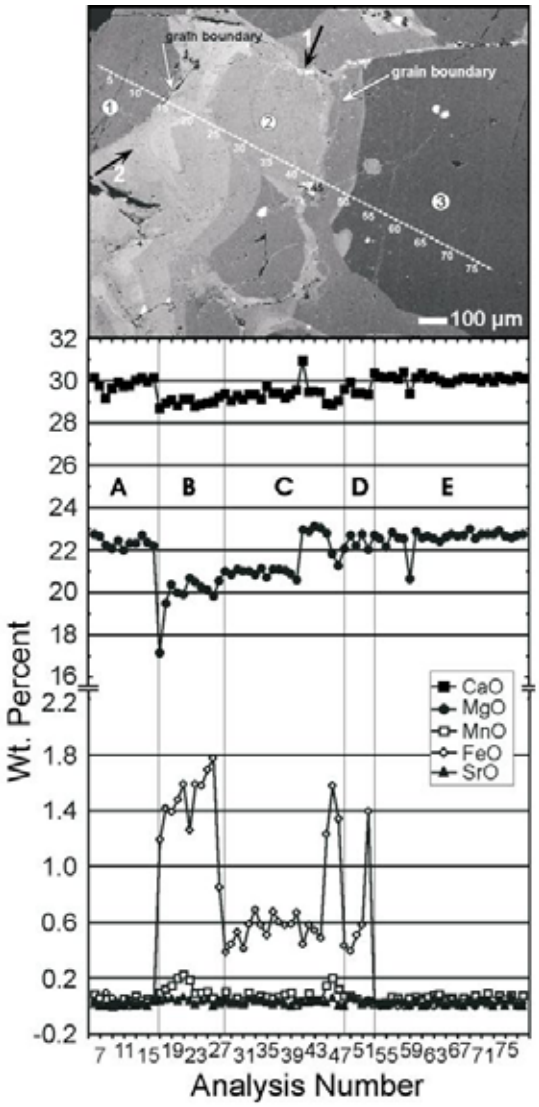

Figure 11: Chemical analysis across the Fe-rich alteration zone between three dolomite grains (labelled 1-3) in the medium-grained dolomite marble of the Corona Formation (Farm Berghof). Grain boundaries are indicated by arrows. The BSE image shows that grain no. 2 is completely altered. The small white grains represent very fine-grained FeS grains. White zones along some grain boundaries (arrow no. 1) represent the highest Fe concentration due to Fe oxidation along the grain boundary. Barium is not shown on the graph because the levels were either extremely low, below the detection limit or showed no definitive correlation to the zonation.

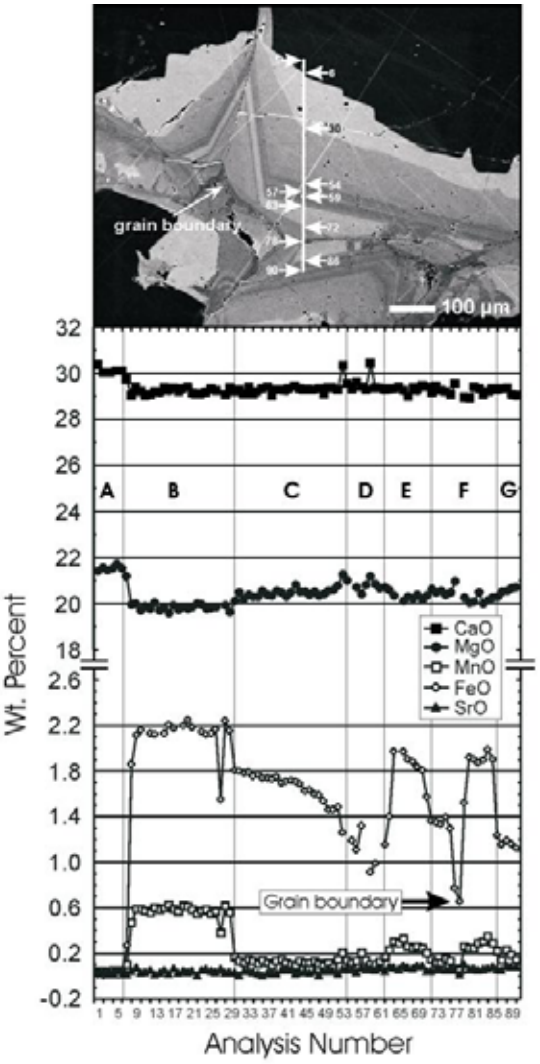

Figure 12:. Chemical profile with corresponding BSE image across an Fe-enriched alteration zone which depicts rhythmical zonations along the grain boundary between two dolomite grains (Corona Formation – Farm Berghof). Numbers indicated on the profile (BSE image) correspond to key positions where significant changes in the Fe and Mn content take place. The anomaly in the FeO and MnO content at point 27 represents measurement error as a result of encountering a scratch in the polished thin section.

FeO content to the right of the grain boundary (area F) is due to reaching the same growth zonation as measured in growth band *E* between analysis points 63 and 72 (Fig. 12).

The MnO content shows a very similar pattern as the FeO content, with the highest MnO values measured in growth band *B*. The only difference appears in the interval between points 30 and 54, where the MnO content does not show a similar trend as the FeO content which decreases towards the rim. SrO remains at very low levels and shows no correlation to the observed zonations. The CaO content is around 30 wt. % in area *A*, and then decreases slightly at the first encounter with the alteration zone. The same pattern is visible in the MgO content, but with a more discernible fluctuation correlated with the introduction of Fe and Mn in the dolomite structure.

One profile with 50 analysis points was made across a sparry dolomite porphyroblast. Changes in the chemical composition were only registered in those areas affected by Fe and Mn fluid infiltration. The luminescent parts of the crystal exhibit the same chemical composition (low Mn and Fe contents) as the medium-grained dolomite marble.

Electron microprobe analyses conducted across the zoned feldspar grains in the Fe-rich zones in the large sparry dolomite porphyroblasts show that although the feldspars are CL-zoned, the composition at all measured

points is close to end-member albite. Na_2O ranges from 11.7 to 12.2 wt.%, for CaO 0.02 to 0.21wt.% and K_2O 0.04 to 0.1 wt.%. The trace elements probably causing the visible CL zonation have such a low concentration that it is beyond the detection limit of the electron microprobe. Ti^{2+} is known to be the activator ion in plagioclase generating blue luminescence colors. However, Ti^{2+} was not detectable with the electron microprobe.

The measured profiles show that the metadolomites are enriched with varying concentrations of iron along the grain boundaries and in mineral grains. Manganese follows a similar enrichment pattern but with a much lower concentration. The enrichment pattern observed in this study confirms previous reports in the literature that the Mn/Fe ratio is important in controlling the luminescence in carbonate rocks (Pierson, 1981; Marshall, 1988). A rise in the FeO content correlates exactly with a rise (although lower in magnitude) in the MnO content.

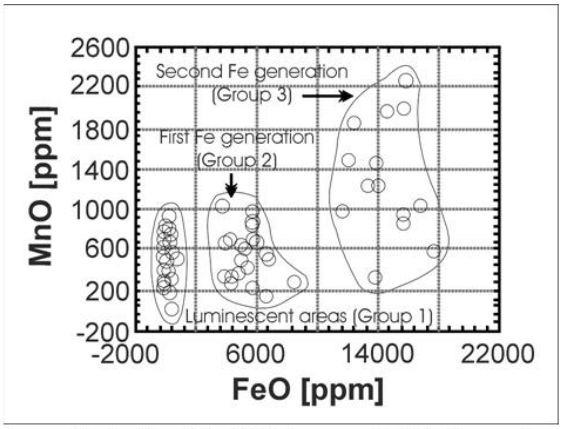

Figure 13: Scatter plot of MnO versus FeO in the medium-grained dolomite matrix. The data correspond to the quantitative line profile in Fig. 11. The three fields correspond to the luminescent cores (Fe-Mn-poor) and to the Fe-Mn-rich grain boundary zonations of the first and second generation.

The FeO and MnO contents can be grouped into three levels of concentration across the unaltered and altered zones along grain boundaries and grain interiors. A plot of Mn versus Fe shows that the zones can be separated out (Fig. 13). The data for this plot corresponds to the microprobe analyses presented in Figure 11. The lowest grouping, generally forming a tight cluster, corresponds to the luminescent regions of the dolomite grains (Group 1). Groups 2 and 3 can be directly correlated to the first and second Fe- and Mn-enriched zones reflecting the two generations of fluid influx, i.e. the two distinct overlapping zonations shown in Fig. 8B. Different profiles across other alteration zones would of course produce different groupings, reflecting the changes in FeO and MnO, but the two fluid influxes would still be discernible.

Discussion

The petrographic analysis has been the most reliable method in characterising the diverse microstructures and grain boundary configurations observable in the graphite-bearing sparry calcite marbles. Grain boundary migration appears to be the dominant mechanism involved in the development of the exaggerated grain growth fabrics. The driving force behind this process is the reduction of interfacial free energies, leading to an increase in the grain size and a reduction of the grain boundary surface area. In the sparry calcite marbles two types of growth can be recognized, normal grain growth and abnormal grain growth, giving rise to a bimodal grain size distribution. The sketch in Figure 14 depicts the development of the fabric at three points in the grain growth process. The starting point for this process begins with an older equilibrium metamorphic grain fabric exhibiting triple-point grain boundaries. A thermal input is necessary for activating boundary mobility in normal grain growth. This has been demonstrated by Buntebarth and Voll (1991) in the Ballachulish contact aureole (Scotland) and Covey-Crump and Rutter (1989)

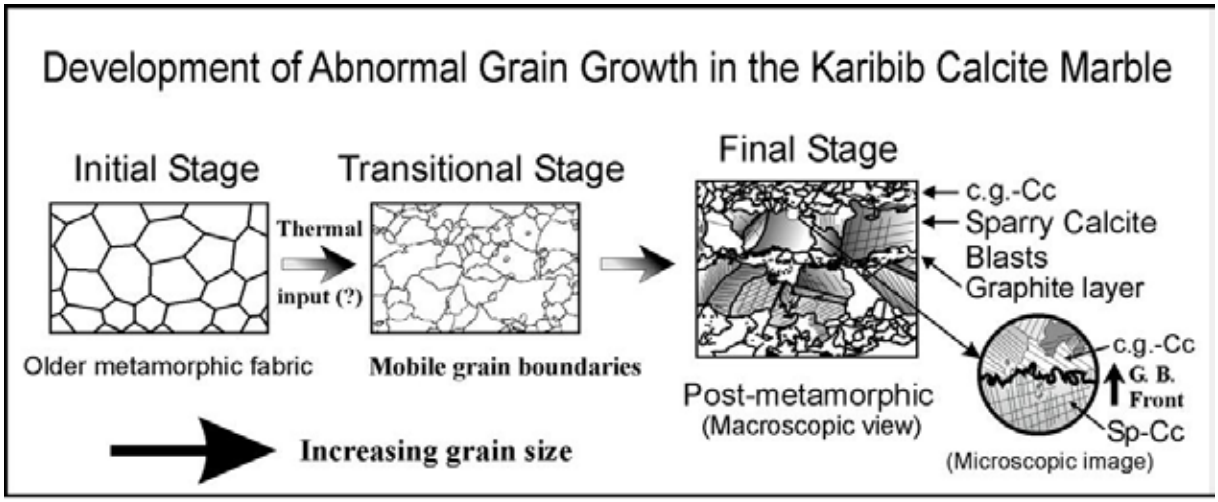

Figure 14: Cartoon sketch depicting the process of fabric development in the graphite-bearing calcite marble with the large sparry calcite rhombohedra (Farm Elim).

in the calcite marbles on Naxos, Greece. Since the CZ of the Damara Orogen is characterised by numerous late- to post-Damara granitic intrusions, the source for the thermal input may be of a regional character.

Initial grain boundary mobility is indicated by the dismantling of triple-point grain boundaries. In the transitional stage (Fig. 14) of the grain coarsening process in the sparry calcite marbles, the original grain boundary configuration has almost disappeared, replaced with irregular and serrated grain boundaries. A few relict equilibrium boundaries are sometimes found. Graphite occurs in nests or along the contacts between calcite grains. In the final stage (Fig. 14), exaggerated grain growth has occurred. This is driven by weak deformation (stored strain energy within the coarse calcite grains) and the decrease in free enthalpy corresponding to the decrease of dislocation density and a further reduction of the grain boundary surface. This post-metamorphic process is a further escalation of the secondary recrystallization that took place in the transitional stage with the formation of the coarse grain fabric. The grain boundaries between the abnormally grown calcite (xenomorphic) and the coarse-grained matrix are irregular (Fig. 14) but the shape of the sparry calcite results from its rhombohedral cleavage. The development of these coarse-grained fabrics are restricted to pure calcite marbles. The presence of impurities or other phases, in this case calc-silicate minerals, hinders the grain coarsening process. Graphite, on the other hand, does not appear to hinder the overall coarsening process in the sparry calcite marbles but only sporadically at the local grain scale. The concentration of graphite in nests and layers substantiates a high mobility.

The extent of fluid activity in the sparry calcite marbles has not been as great as compared to the sparry dolomite marbles and associated metacarbonates. Generally homogenous CL colours are found. Zonation microstructures only occur where the sparry calcite marbles have been affected by the later cataclastic deformation. This does not mean, however, that the exaggerated grain growth fabrics developed under dry conditions. Experimental work by Tullis and Yund (1982) have shown in quartz, for example, that the addition of water along the grain boundaries increases the solubility. Transfer rates or flux increases occur from one grain to another by increasing the concentration of Si in the intergranular fluid (Tullis and Yund, 1982). In calcite, the rate of grain growth is much faster in the presence of a CO_2 and H_2O fluid and, thus, the presence of a grain boundary fluid phase may have aided the grain growth process in the sparry calcite marble.

The CL observations, BSE imaging and the electron microprobe results all indicate that a complex series of events, resulting from hydrothermal fluid infiltration, led to the development of the observed structures and fabrics in the metadolomites of the Corona Formation. The formation of the large sparry dolomites is not as clear cut as the development of the sparry calcite fabrics by grain boundary migration. Only at higher temperatures does dolomite exhibit indications of grain boundary migration and the temperature data from Puhan (1995) shows that medium-grade conditions prevailed. Furthermore, dolomite has physical properties different from those of calcite, and thus reacts differently to the same physical conditions. Grain growth processes such as those ascribed to Ostwald ripening may not apply here. The development seems to be related to a complex interaction of solid-state and hydrothermal processes. Incorporation of matrix grains into the sparry dolomite is visible at the interface zone between the matrix and the sparry dolomite. In the margin area, subgrains can also be observed with small misorientations. These observations suggest that solid state process were active during grain growth. The CL fabrics in the sparry dolomite are indicative of fluid infiltration. However, the growth of the sparry dolomite porphyroblast by coalescence crystallization is interpreted to be younger than the Fe-/Mn-rich zonations parallel the grain boundaries in the dolomite matrix. The fine network of Fe-stained microstructures (visible by CL and enhanced by etching) outline the former grain boundaries of the matrix dolomite grains that were incorporated into the growing sparry dolomite. In other words, the visible CL fabrics in the sparry dolomite are preserved relicts, since the solid state crystallization incorporated the Fe-rich zoning and did not destroy it. On the other hand, another possibility also needs to be considered which suggests that the sparry dolomite porphyroblasts are older than the Fe-rich fluid infiltration. Fe-rich fluid pathways of the dominant second generation are found cross-cutting the sparry dolomite crystal, which are also connected to the Fe-rich grain boundary zonations in the matrix. Such cross-cutting relationships suggest that sparry dolomite is older.

Fluid participation is quite prevalent during faulting and is associated with hydrothermal mineralisation (Sibson, 2000). Regional fieldwork in the SMZ of the Damara Belt shows that the grain growth in the sparry dolomite marbles only occurs where hydrothermal processes are observed. They also appear to be fault-bounded occurrences. This is evident in an approximately 300 km long and ca. 20 km wide zone which strikes NE to the Damara Orogen. It can be followed from the Kammberg on the margin of the Namib Desert through Gamsberg, Naos, Dordabis and up to Witvlei.

The CL microstructures which have been documented in the medium-grained dolomite matrix and the associated metacarbonate rocks are characterised by diffusion zonation, growth zonations exemplified by concentric zoning and zonal structures transecting grain boundaries in the Fe alteration zones, and irregular oscillatory zoning representing reprecipitation in voids formed by preceding corrosion. This led to a wide array of alteration and CL fabrics in the metadolomites. Hydrothermal fluids of changing composition reacted with the distinct mineralogical compositions of each rock type.

Distinct generations of Fe-bearing fluid migration are discernible in the metadolomites. Two easily recognisable generations of Fe-rich zonations parallel the grain boundaries in the medium-grained sparry dolomite marble (Fig. 8B). An interconnected network becomes immediately apparent. Age relationships between the two phases of Fe-rich fluid influx can be determined. The migration of Fe-rich fluids are not uniformly distributed between the two fluid generations. The type of enrichment pattern produced in the sparry dolomite marble could be interpreted as reflecting episodic fluid influx during the alteration of the Corona Formation. What the causes or reasons for the fluctuations are is at present unknown, but a type of hydraulic pumping related to seismic events could be a possibility (Sibson *et al.*, 1975).

The development of the unique alteration features visible in the metadolomites (using the medium-grained sparry dolomite matrix as an example) are shown in the simplified model in Figure 15. Stages of development are not necessarily separated in time but may represent transitional processes during the overall hydrothermal alteration. The stages are defined by changes in the fluid chemistry.

The starting material consists of a metadolomite exhibiting a mosaic rock fabric (Stage I). Intergranular Fe-/Mn-bearing fluids infiltrate the rock during hydrothermal alteration (Stage I) and migrate along grain boundaries and microcracks. Diffusion of Fe and Mn from the grain boundaries and microcracks into the grains lead to the first generation of Fe and Mn alteration. Introduction of Fe into the grain probably occurred rapidly, since the highest Fe concentration occurs at the innermost zonation boundary, and then begins to progressively decrease towards the grain boundary. Hydraulic pumping in the system promotes the development of a second generation richer in Fe (Stage I) and results in the stronger CL quenching zonations overlapping the first generation (Fig. 15). Changes in the grain boundary configuration by minor dissolution probably occurs but the extent of Fe and Mn enrichment into the dolomite grains results predominantly through diffusion.

Changes in the system (decreasing temperature) occur in Stage II. This leads to solution and the creation of large pore spaces (hatched area in Fig. 15). Both the first and second generation of the Fe-rich zones are affected by the solution, as well as the original unaltered grains. Precipitation of carbonate material occurs in the voids in Stage III where cyclical fluid influx leads to changes in composition which produces the rhythmic growth zones depicted in Figure 15 and in the BSE image of Figure 12.

The last phases in the formation of the fabric are represented by Stages IV-V in Figure 15. During these stages a corrosive event leads to the total destruction of the Fe-rich network, growth zones and parts of the unaltered dolomite grains. Precipitation of fine-grained to coarse-grained generations of dolomite with a CL fabric displaying Fe-rich and Fe-poor grains takes place in these voids and also occurs as a total replacement of the former grain fabric (stippled area in Fig. 15).

Acknowledgements

This research was supported by the Deutsche Forschungsgemeinschaft within the framework of the SFB 468: "Interactions at Geological Interfaces", University of Göttingen. The authors also wish thank the reviewers for their helpful comments on an earlier draft of this paper.

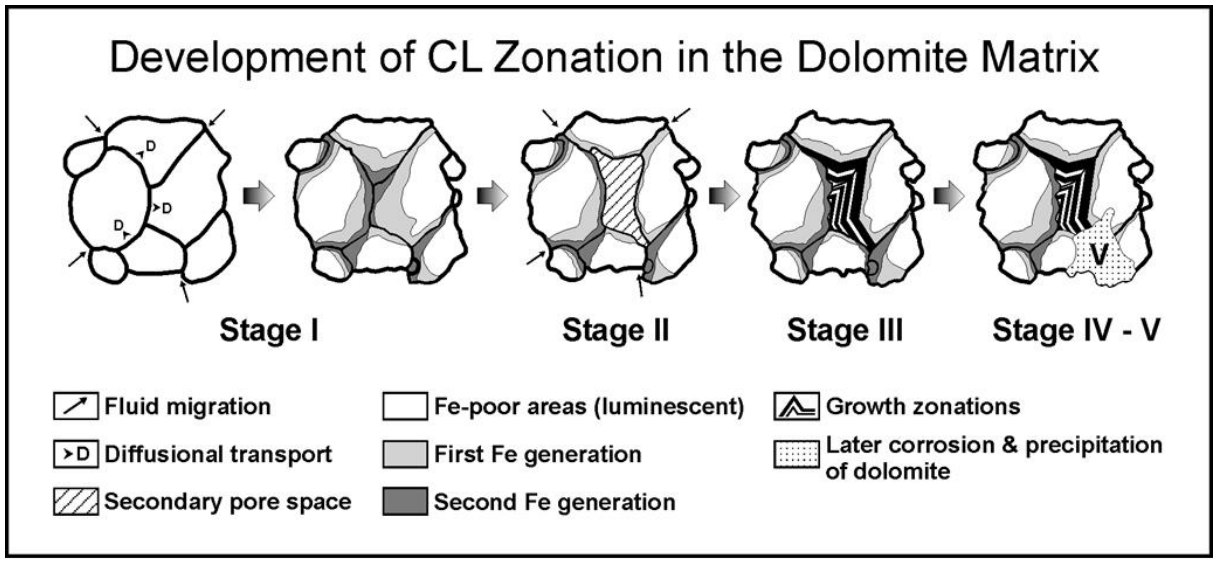

Figure 15: Simple model showing the interpretation for the Fe-rich zones visible along the grain boundaries in the medium-grained dolomite marble (Corona Formation – Farm Berghof). Five stages occurred in the process, with the final fabric depicted in Stage IV -V.

References

Barker, C.E. and Kopp, O.C. 1991. Luminescence microscopy and spectroscopy: qualitative and quantitative applications. *SEPM, Short Course*, **25**, 95 pp.

Buntebarth, G. and Voll, G. 1991. Quartz grain coarsening by collective crystallization in contact quartzites, *In*: Voll, G., Töpel, J., Pattison, D.R.M. and Seifert, F. (eds) *Equilibrium and kinetics in contact metamorphism*. Springer-Verlag, Heidelberg, 251-265.

Covey-Crump, S.J. and Rutter, E.H. 1989. Thermally-induced grain growth of calcite marbles on Naxos Island, Greece. *Contrib. Mineral. Petrol.*, **101**, 69-86.

Detert, K. 1978. Secondary recrystallization. *In*: Haessner, F. (ed.) *Recrystallization of Metallic Materials*. Riederer, Stuttgart, 97-110.

Gross, C.J., Weber, K., Vollbrecht, A. and Siegesmund, S. 1999. Cathodoluminescence and electron microprobe study of dolomitic marbles from Namibia: Evidence for hydrothermal alteration. *Z. dt. geo. Ges.*, **150**, 333-357.

Henry, G., Clendenin, C.W., Stanistreet, I.G. and Maidin, K.J. 1990. Multiple detachment model for the early rifting stage of the Late Proterozoic Damara Orogen in Namibia. *Geology,* **18**, 67-71.

Hillert, M. 1965. On the theory of normal and abnormal grain growth. *Acta Metall.*, **13**, 227-238.

Klein, J.A. 1980. Geological report on area 2115A. *Unpubl. Rep. geol. Survey S. W. Afr./Namibia*, 25 pp.

Kingery, W.D., Bowen, H.K. and Uhlmann, D.R. 1976. *Introduction to Ceramics*. Wiley, New York, 1032 pp.

Marshall, D.J. 1988. *Cathodoluminescence of Geological Materials*. Unwin Hyman, Boston, 143 pp.

Miller, R.McG. 1983. The Pan-African Damara Orogen of South West Africa/Namibia, 431-515. *In*: Miller, R.McG. (ed.) *Evolution of the Damara Orogen of South West Africa/Namibia*. Spec. Publ. geol. S. Afr., **11**, 515 pp.

Neuser, R.D., Bruhn, F., Habermann, D., and Richter, D.K. 1995. Kathodolumineszenz: Methodik und Anwendung. *Zbl. Geol. Paläont., Teil I*, **1/2**, 287-306.

Pierson, B.J. 1981. The control of cathodoluminescence in dolomite by iron and manganese. *Sedimentology,* **28**, 601-610.

Porter, D.A. and Easterling, K.E. 1981. *Phase transformations in metals and alloys*. Van Nostrand Reinhold Company, New York, 446 pp.

Puhan, D. 1983. Temperature and pressure of metamorphism in the central Damara Orogen, 219-223. *In*: Miller, R.McG. (ed.) *Evolution of the Damara Orogen of South West Africa/Namibia*. Spec. Publ. geol. Soc. S. Afr., **11**, 515 pp.

Puhan, D. 1988. Reverse age relations of talc and tremolite deduced from reaction textures in metamorphosed siliceous dolomites of the southern Damara Orogen (Namibia). *Contrib. Mineral. Petrol.*, **98**, 24-27.

Puhan, D. 1995. Metamorphic evolution of the assemblage tremolite + talc + calcite + dolomite + quartz within a sample of siliceous dolomite from the southern Damara Orogen (Namibia). *Contrib. Mineral. Petrol.*, **120**, 180-185.

Reed, S.J.B. 1996. *Electron microprobe analysis and scanning electron microscopy in geology*. Cambridge University Press, Cambridge, 201 pp.

Sibson, R.H., Moore, J.McM. and Rankin, A.H. 1975. Seismic pumping – a hydrothermal fluid transport mechanism. *J. geol. Soc. London*, **131**, 653-659.

Sibson, R.H. 2000. Fluid involvement in normal faulting. *J. Geodynamics*, **29**, 469-499.

Stöckhert, B. and Duyster, J. 1999. Discontinuous grain growth in recrystallized vein quartz – implications for grain boundary structure, grain boundary mobility, crystallographic preferred orientation and stress history. *J. struct. Geol.*, **21**, 1477-1490.

Tullis, J. and Yund, R.A. 1982. Grain growth kinetics of quartz and calcite aggregates. *J. Geol.*, **90**, 301-318.

Ullemeyer, K., Spalthoff, P., Heinitz, J., Isakov, N.N., Nikitin, A.N. and Weber, K. 1998. The SKAT texture diffractometer at the pulsed reactor IBR-2 at Dubna: experimental layout and first measurements. *Nuclear Instruments and Methods in Physics Research*, **A 412**, 80-88.

Weber, K. and Vietor, T. 1996. *Höffigkeitsbewertung geophysikalischer Anomalienmuster in Namibia*. Unpubl. Abschlußbericht zum Hochschulvergabeprojekt der Bundesanstalt für Geowissenschaften und Rohstoffe, Hannover, 89 pp.